Templating of cylindrical and spherical block copolymer microdomains by layered silicates

Adriana S. Silva[a] and Cynthia A. Mitchell
Department of Chemical Engineering, University of Houston, Houston, Texas 77204-4004

Mun Fu Tse and Hsien-C. Wang
Baytown Polymer Center, Exxon Mobil Chemical Company, Baytown, Texas 77521

Ramanan Krishnamoorti[b]
Department of Chemical Engineering, University of Houston, Houston, Texas 77204-4004

(Received 1 March 2001; accepted 24 July 2001)

The influence of a highly anisotropic layered silicate (organically modified montmorillonite) in directing the mesoscopic self-assembly of a block copolymer blend is studied as a model for the development and tailoring of templated inorganic–organic hybrid materials. The potential for nanometer thick layers to induce large-scale mesoscopic ordering of cylindrical and spherical microdomains in asymmetric block copolymers is studied using a combination of rheology, electron microscopy, and small angle neutron scattering. Spherical microdomains arranged on a bcc lattice are templated by the anisotropic layered silicate and the kinetics of their growth are dramatically accelerated by the presence of even 0.1 wt.% (0.04 vol.%) of the filler. However, for cylindrical microdomain ordering, the kinetics are essentially unaffected by the addition of layered silicates and the development of three-dimensional mesoscopic order is possibly even disrupted. These results suggest that for the development of three-dimensional well-ordered nanostructures, the surface defining the pattern has to be significantly larger than the leading dimension of the structure being templated. © *2001 American Institute of Physics.* [DOI: 10.1063/1.1403003]

INTRODUCTION

Block copolymers are capable of forming a rich range of nanostructures depending on the relative chain lengths, constituent chemical species, and architecture of its components.[1] The mechanism of nanostructure development in such microphase segregated systems, resulting from the thermodynamic incompatibility of covalently linked blocks, is of considerable interest because they can serve as model systems to understand the self-organization of surfactants[2] and vesicle systems.[3] We report in this study the effect of adding a highly anisotropic nanometer thick layered silicate on the mesoscopic ordering of a triblock/diblock copolymer blend to either hexagonally packed (HEX) cylinders or body-centered cubic (bcc) spheres.

Molecularly mixed inorganic–organic templated hybrids[4] have the potential for the development of a new generation of materials that are of significant interest to catalysis, size- and shape-selective membranes, lightweight structural composites, and barrier materials.[5] While surfactants and block copolymers have been used to template the growth of inorganic mesophases,[6] and mesoporous silica has been recently used to fabricate nanofibers of linear polyethylene by extrusion polymerization,[7] we use the *inorganic* phase (layered silicate) as the templating agent for the development and careful control of mesoscopic order in a block copolymer blend.

Structurally, three broad classes of nanocomposites are achievable based primarily on the strength of the polymer–silicate interaction: immiscible or demixed macrocomposites, intercalated nanocomposites, where the layer registry is maintained with a swollen interlayer gallery, and finally delaminated hybrids, where the individual layers of layered silicate are dispersed in a polymer matrix (Fig. 1). In this work, the nanocomposite created belong to the intercalated class of hybrids.

We examine a blend of a matched triblock polystyrene–poly(ethylene-butene-1)–polystyrene (PS–PEB–PS) and its corresponding PS–PEB diblock copolymer, capable of exhibiting thermally driven order–order and order–disorder transitions. The nanometer thick, highly anisotropic filler used here belongs to the smectite family of 2:1 layered silicates, namely montmorillonite. This naturally occurring layered silicate (a disk of thickness 0.95 nm and diameter 0.5–1 μm) was modified with dimethyl–dioctadecyl ammonium and exhibits a slight preferential attraction to the polystyrene block. We exploit the large surface area per unit volume of the nanometer thick sheetlike layered silicates[8] to provide a templating agent for the block copolymer blend ordering onto bcc lattice based spherical and hexagonally packed cylindrical microdomains. In particular, by using a block copolymer blend system exhibiting a thermally driven order–order transformation from cylinders to spheres,[9–11] we examine the influence of the organically modified montmorillonite on the growth mechanism of cylindrical and spherical microdomains without any additional perturbations to the system. We note in passing that the addition of 3 wt. % or

[a]Present address: Corporate R&D, Materials Sciences, The Dow Chemical Company, Freeport, Texas 77541.
[b]Author to whom correspondence should be addressed. Electronic mail: ramanan@mail.uh.edu

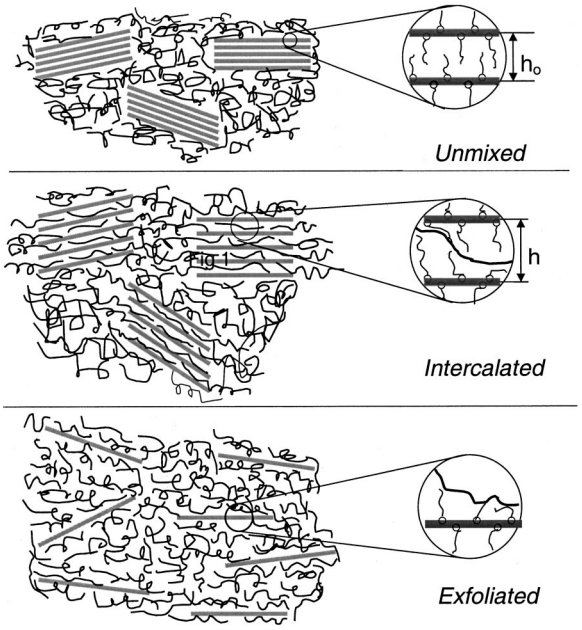

FIG. 1. Schematic of the three thermodynamically achievable nanostructures for polymer layered-silicate hybrids (Ref. 18). The immiscible system represents conventional talc-based macrocomposites. The hybrids studied in this work are intercalated hybrids with occasional individual layers separated from the tactoids, with each tactoid typically consisting of 5 to 30 layers.

less of the layered silicate (2C18M) has negligible influence on the location of the order–disorder and order–order transitions. By varying the amount of the layered silicate, we examine the effect of its addition on the kinetics of the cylinder to sphere order–order transition starting from unaligned cylinders and shear-aligned cylinders, allowing us to verify the requirement of a well-defined three-dimensional structure in controlling the growth of ordered spherical microdomains. A complementary study on the effect of the nanoparticle size on the kinetics of block copolymer blend ordering is presented in the accompanying paper.[12]

EXPERIMENT

The block copolymer used in this study is a blend of a triblock polystyrene (PS)–poly(ethylene-co-butene-1) (PEB)–polystyrene (PS) and its matched diblock copolymer (Kraton G 1657 from Shell Chemical Co., used as received).[9–11] The phase behavior, morphology, and linear viscoelastic behavior, along with the characterization of the order–order and order–disorder transitions, have been reported previously.[9–11] The unfilled block copolymer blend forms cylindrical microdomains of PS at low temperatures, with a diameter of ~27 nm and several microns long. At temperatures above the order–order transition ($T_{OOT}=138\pm3\,^{\circ}C$), the block copolymer blend forms spherical microdomains of PS with a diameter of ~23 nm arranged on a bcc lattice. At higher temperatures, the block copolymer blend disorders, with an order–disorder transition temperature (T_{ODT}) of $195\pm5\,^{\circ}C$[9–11] (see the Appendix).

The organically modified layered silicate is a dimethyl–dioctadecyl ammonium substituted montmorillonite (2C18M), with a CEC of 90-meq/100 g and characterized extensively in a previous paper.[13] Each individual silicate layer can be considered to be a disk with thickness 0.95 nm and diameter ranging from 0.5 to 1 μm. The reported diameter of montmorillonite is a best estimate based on electron micrographs of a wide range of polymer nanocomposites that indicate the presence of a distribution of diameters that are thought to arise because of the edge–edge and edge–face aggregation, flexibility of the layers, and the intrinsic inhomogeneity of these natural layered materials. Nanocomposites were prepared by solution mixing appropriate quantities of finely ground 2C18M (0.1, 1, and 3 wt.%) and the block copolymer blend in toluene at room temperature. The homogeneous solutions were dried extensively at room temperature and subsequently annealed at 100 °C in a vacuum oven for ~12 h to remove any remaining solvent and to facilitate complete polymer intercalation between the silicate layers. X-ray diffraction was used to verify the gallery height and was performed using a Siemens D5000 x-ray diffractometer with Cu–K_α radiation generated at 40 mA and 50 kV. Diffraction spectra were obtained over a 2θ range of 2° to 10° in steps of 0.02° and counting times of 3 s at each angular position.

Melt state viscoelastic measurements were performed using a Rheometrics ARES rheometer with 25 mm diam parallel plates and a transducer with an operating range of 0.2–2000 g cm. Samples of ~2 mm thickness were vacuum molded at 180 °C for 30 min using a 1 ton load in a Carver press. After loading the sample in the rheometer, it was heated to 220 °C under a N_2 blanket and held there for approximately 30 min in order to erase all prior thermomechanical history before cooling to a temperature below T_{ODT}. While cooling or heating the sample in the ordered state, it was always ensured that the normal force was close to zero, so as not to induce any macroscopic alignment of the sample.

The kinetics of the order–order and the disorder–order transition were followed by monitoring the low-frequency linear viscoelastic oscillatory shear properties (storage and loss moduli, G' and G'', respectively) as a function of time at constant strain amplitude γ_0, frequency ω, and temperature T. Typically, the sample reached thermal equilibrium in less than 10 min following a temperature jump. The conditions of ω and γ_0 were carefully selected to ensure a linear viscoelastic response with little or no changes in the microstructure as a result of the rheological testing, a torque signal that was considerably larger than the instrumental resolution, and a sampling time that was short but not at the cost of compromising the sensitivity of the kinetic data. On the other hand, shear alignment of the cylindrically ordered block copolymers were performed by the application of large-amplitude oscillatory shear at $T=120\,^{\circ}C$ at $\omega=0.01$ rad/s and $\gamma_0=100\%$ for a time of ~24 h. The viscoelastic signatures were verified to be time independent, ascertaining complete alignment and ensuring that the sample did not suffer melt fracture by the prolonged application of large-amplitude shear.

Samples for transmission electron microscopy were removed from the rheometer after rheological measurements

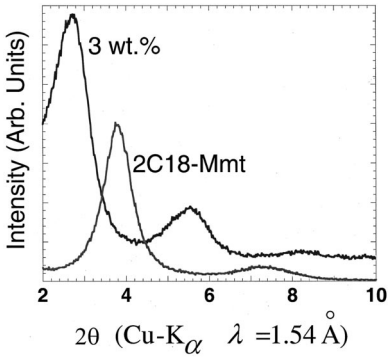

FIG. 2. X-ray diffraction spectra for the pure 2C18M and the 3 wt.% hybrid. The ⟨001⟩ and ⟨002⟩ peaks, corresponding to the midplane to midplane distance of the layered silicate, are shifted to smaller diffraction angles for the hybrid, indicating the intercalation and hence swelling of the interlayer galleries. The gallery heights were calculated using Bragg's law ($\lambda = 1.54$ Å), the measured value of $2\theta_{001}$, and the known thickness of the individual silicate layers of ~9.5 Å.

and cooled rapidly (in liquid nitrogen or cold water) so as to preserve the microstructure of the test conditions. These samples were cryomicrotomed at −130 °C to obtain ultrathin sections (<100 nm thick) for TEM. These sections were stained with RuO_4 (a stain preferentially taken up by PS) and then examined using a 160 keV Phillips EM 300 TEM, as described earlier.[14]

SANS measurements were performed on the 30 m SANS beamline (NG3) at NIST, Gaithersburg, MD. Neutrons with wavelength (λ) of 6 Å and Δλ/λ of 0.15 were used with sample to detector distances ranging from 5 to 6.5 m. Quiescent experiments were performed by placing a 1 mm thick sample in a 17 mm annulus sandwiched between two quartz windows and heated in a sealed oven. All quiescent experiments were performed by heating to the isotropic state and then quenched to 162 °C and allowing to equilibrate for ~24 h and the data after correction for background and empty cell scattering were placed on an absolute scale by calibrating with secondary standards. Shear experiments were performed with a 0.5 mm thick sample loaded in an aluminum shear cell and placed in the *in situ* reciprocating shear device developed by Bates and co-workers.[15,16] The temperature of both sides of the shear cell was independently controlled to within ±1 °C and had a rapid response insofar as the heating was concerned. The neutron beam was parallel to the velocity gradient direction ($\nabla \mathbf{v}$). Reciprocating steady shear experiments with one of the plates held stationary and the other undergoing a strain amplitude of 200% with a strain rate $|\dot{\gamma}|$ of 10 s^{-1} were performed. Corrections to the shear cell based SANS data due to the empty cell and background scattering have not been applied and the intensities are not calibrated with a secondary standard.

RESULTS AND DISCUSSION

Structure and dispersion

X-ray diffraction spectra for 2C18M and a representative intercalated hybrid are shown in Fig. 2. The interlayer gallery height of the well-ordered intercalated stack, calculated as the difference of the d_{001} distance obtained by x-ray diffraction and the individual layer thickness of 9.5 Å expands from 13.5 Å for the 2C18M to 21.5 Å for the hybrid, suggesting infiltration of the interlayer galleries by the block copolymer blend. Previous studies have demonstrated that pure PEB is immiscible with 2C18M, while homopolymer PS forms an intercalated hybrid with 2C18M with a gallery height of 21.5 Å.[13,17] This thermodynamic preferential behavior by PS as compared to PEB toward the silicate layers is consistent with the theories of intercalation suggested by Vaia and Giannelis[18] and Balasz and co-workers.[19] However, as demonstrated in a previous paper, this preferential attraction of PS to the silicate surface does not imply that the PEB block is excluded from the interlayer galleries.[13] On the contrary, it has been demonstrated that, on the basis of the relative rigidity of the silicate layers and the relative sizes of the polymer chains (even in their extended conformations) and the silicate layers, the PEB block has to enter the interlayer gallery.

The structure of the nanocomposite as determined by transmission electron microscopy (TEM) of the hybrids (shown in the accompanying paper), reveals stacks of 6–15 intercalated silicate layers with the occasional presence of individual highly anisotropic layers separated from the stacks.[12] We note that individual silicate layers are ~1 nm thick with irregular lateral dimensions of 0.5–1 μm and a surface area of ~800 m^2/gm (if fully exfoliated). The preferential attraction of the PS block to the large surface area of the highly anisotropic silicate layers is primarily responsible for the potential to develop mesoscopically templated nanostructures, as shown below.

Ordering kinetics

For the low levels of layered silicate used to prepare the hybrids reported in this paper, the location of thermal phase transitions, i.e., T_{OOT} and T_{ODT}, as studied by SANS and linear viscoelastic measurements are essentially unaffected by the addition of the layered silicate (with changes less than 1 °C).[20] Additionally, as shown in the Appendix, the blending of the matched diblock and triblock does not have a dramatic influence on the phase behavior. Further, since the volume fraction of added silicate is less than 0.02 in these studies, preferential segregation of the diblock or the triblock to the surface cannot be responsible for the observed behavior. As a matter of protocol, consistent with our previous studies for the unfilled block copolymers,[9–11] samples are quenched from the disordered state (220 °C) to either 150 °C to obtain bcc spherical ordering, or to 120 °C to obtain cylindrical microdomain ordering.

The development of cylindrical and spherical order in the block copolymer blend is conveniently probed using low-frequency isochronal linear viscoelastic measurements, as a result of the large change in the viscoelastic moduli at low frequencies during the ordering process. Previous work has shown that the kinetics inferred from the low-frequency viscoelastic moduli, particularly the storage modulus G', are consistent with those obtained from x-ray scattering and microscopy.[9–11,21,22] In this work, we focus on the storage modulus, as it is the most sensitive rheological tool to observe the ordering phenomenon.

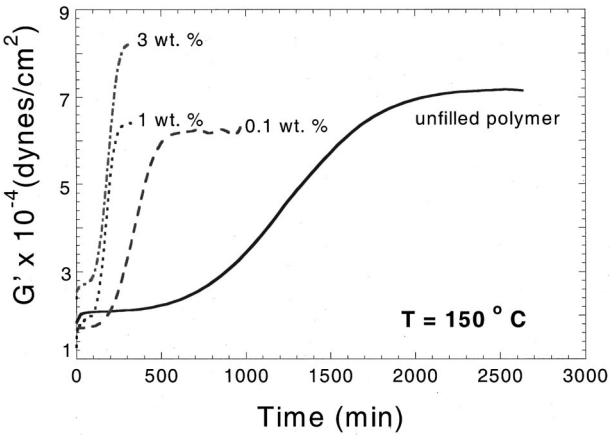

FIG. 3. Temporal evolution of the storage modulus (G') ($\omega = 0.03$ rad/s, $\gamma_0 = 0.015$) for the growth of spherical microdomains at 150 °C from an initial disordered state at 220 °C for the unfilled and filled systems. The sample is thermally equilibrated to within ±0.1 °C within 10 min. Significantly enhanced ordering kinetics are observed for the 0.1 wt.% (0.04 vol.%) hybrid thought to result from the templating of the spherical microdomains by the highly anisotropic layered silicate.

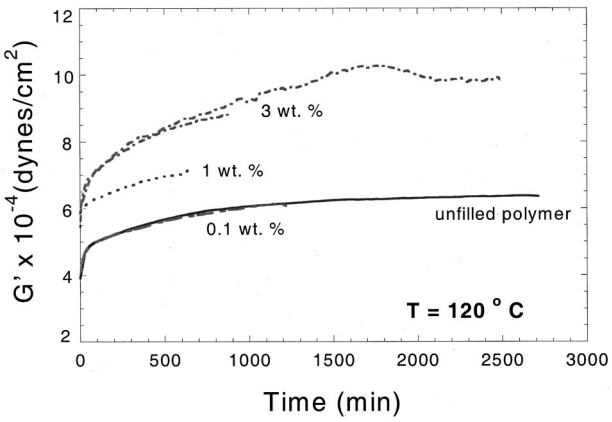

FIG. 4. Temporal evolution of the storage modulus (G') ($\omega = 0.01$ rad/s, $\gamma_0 = 0.015$) for the growth of cylindrical microdomains at 120 °C from an initial disordered state at 220 °C for the unfilled and filled hybrids. The kinetics are essentially unaffected by the presence of the layered silicate, with a possibility of slight slowing for the 3 wt.% hybrid. Two sets of data for the 3 wt.% hybrid are recorded and shown here to demonstrate the reproducibility of the data.

The development of the bcc spherical microdomain structure, as monitored by G' for a temperature jump to 150 °C from a disordered state at 220 °C, is shown in Fig. 3. The unfilled polymer exhibits the characteristic sigmoidal growth[21,23] and takes ~2400 min to fully develop.[9–11] The addition of *even minute amounts* of the layered silicate nanolayers (2C18M) results in a dramatic acceleration of the ordering kinetics—taking only ~600 min to fully develop for a 0.1 wt.% (0.04 vol.%) hybrid and ~250 min to develop for the 1 and 3 wt.% hybrids. There is no appreciable difference in the kinetics of the 1 and 3 wt.% sample (in fact, being invariant for even a 10 wt.% hybrid and not shown in this study), with only an increase in the magnitude of the modulus, as expected for higher filler loading.[24] This dramatic acceleration of the kinetics for hybrids is attributed to the *nucleation and templating* influence of the highly anisotropic, large surface area filler on the development of spherical microdomains, whose diameter (~23 nm) is considerably smaller than the lateral dimensions of the silicate layers (diameter ~0.5–1 μm). The rapid saturation of the templating effect of the filler (the kinetic effect saturating for filler loadings of ~1 wt.%) is thought to arise as a result of the large surface area associated with the silicate layers and a saturation of the nucleation sites for the preferential PS segments of the block copolymer blend at extremely low loadings.

In contrast, as shown in Fig. 4 the kinetics for the development of cylindrical microdomains (at 120 °C) from an initial disordered state (at 220 °C) are essentially unaffected by the addition of the layered silicate. In fact, the time dependence of G' (at early times) for the 3 wt.% hybrid is *slightly* weaker than that of the unfilled polymer and *might suggest* that the silicate layers *hinder* the development of the cylindrical structure. In the *unfilled* polymer, the micron length cylindrical microdomains when grown at 120 °C, arrange themselves in a three-dimensional hexagonal array, a geometry that would not be easily templated by nanometer thick layers with irregular lateral structure and diameters that are submicron and smaller than the length of the cylinders.[9,13,25] The PS block forming the cylindrical microdomains is preferentially attracted to the silicate surface, suggesting the possibility of developing long-range correlations between the PS microdomains and enhanced kinetics for the growth of cylindrical microdomains. However, the ceramic layered silicates are considerably stiffer and shorter than the block copolymer cylinders (but considerably longer than a single extended chain), and thus even slight imperfections in the relative orientations of the silicate layers or bending of the silicate layers, results in a disruption of the long-range correlations of the cylindrical microdomains (Fig. 5).

To further verify the importance of a three-dimensional scaffold structure in the development of spherical microdomains arranged on a bcc lattice, we exploit the thermotropic cylinder to sphere transition exhibited by the copolymer blend system. The cylindrically ordered microdomains un-

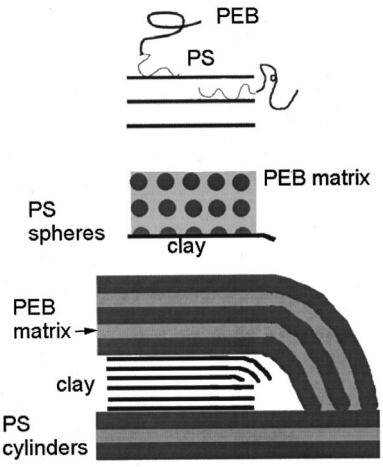

FIG. 5. A schematic representation of the preferential attraction of the PS block to the silicate layers and the potential for the development of well-oriented spherical microdomains and the disruption of the cylindrical microdomain ordering due to the silicate layers.

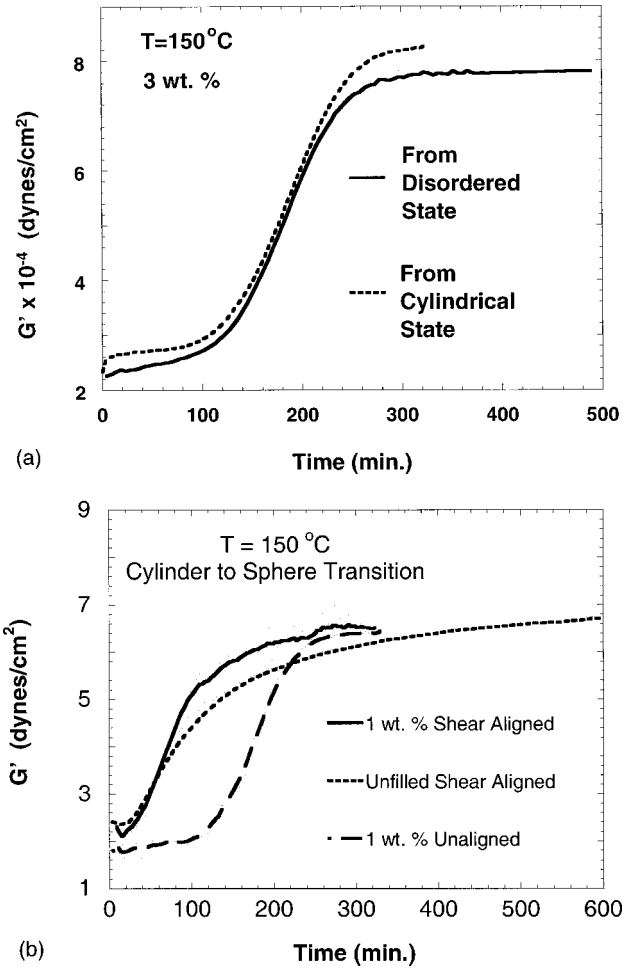

FIG. 6. Temporal evolution of the storage modulus (G') (with $\omega = 0.03$ rad/s, $\gamma_0 = 1.5\%$): (a) for the development of spherical microdomains at $T = 150$ °C from an initial disordered (220 °C) state and macroscopically unaligned cylindrical microdomain structure (120 °C) for a 3 wt.% 2C18M-based nanocomposite; and (b) for the development of spherical microdomains at $T = 150$ °C from macroscopically unaligned cylindrical microdomain structure and a shear-aligned cylindrical structure at 120 °C for a 1 wt.% 2C18M-based nanocomposite. Additionally, in (b) the transformation kinetics for the unfilled polymer starting from a shear-aligned cylindrical structure to the spherical state is shown. Samples were shear aligned in the cylindrical state by prolonged application (~24 h) of large-amplitude oscillatory shear at $T = 120$ °C using a strain amplitude γ_0 of 100% at a frequency of $\omega = 0.01$ rad/s.

dergo a thermotropic transformation to spherical microdomains when heated to temperatures above $T_{OOT}(=138 \pm 3$ °C).[9–11] Starting from unoriented cylindrical microdomains, grown under quiescent conditions (i.e., no macroscopic orientation of the cylindrical microdomains, with the microdomain grains being randomly oriented), the transformation to spherical microdomains arranged on a bcc lattice as studied by linear viscoelastic measurements are shown in Fig. 6(a). These kinetics, like those of the unfilled polymer, are identical to the development of spheres from the disordered state [Fig. 6(a)].[9,11,12] Previously, we have shown that the transformation of unaligned cylindrical microdomains to spherical microdomains arranged on a bcc lattice is mediated by a poorly ordered state exhibiting liquidlike viscoelastic and SANS signatures.[9,11] This pathway appears to be unchanged by the addition of the nanoscale fillers, where the presence of the silicate layers might have been anticipated to stabilize the ordered phases and discourage the formation of the liquidlike intermediate state.

Further, macroscopically aligned cylinders in the *unfilled* polymer, prepared by the prolonged application of large-amplitude oscillatory shear at $T = 120$ °C, exhibit accelerated kinetics for the transition to a spherical microdomain state when heated to 150 °C.[10] The transformation of shear-aligned cylinders to spheres, while passing through an intermediate poorly ordered state, results in an epitaxial development of the spheres with the arrangement of the spherical microdomains exhibiting memory of the initial orientation of the aligned cylindrical microdomains (as shown below). These kinetics for the shear-aligned cylinder to sphere transition are unaffected by the addition of 1 wt.% of the layered silicate, as shown in Fig. 6(b), suggesting that the existence of a well-defined three-dimensional scaffold enhances the development of the bcc spherical microdomains. These reinforce our earlier argument that the preferential attraction of the PS block to the silicate surface and the resulting long-range templating of the structure are responsible for the faster kinetics of spherical microdomain growth in the filled hybrids.[26]

Direct confirmation of this is obtained from the small angle neutron scattering (SANS) measurements on *in situ* shear-aligned samples[15] and the results are presented in Fig. 7. The two-dimensional SANS data in Figs. 7(a) and 7(b) confirm the epitaxial relationship between the block copolymer blend cylinder axis and the $\langle 111 \rangle$ axis of the spheres arranged on a bcc lattice. Shear alignment of the cylinders leads to the development of ''parallel'' cylinders (with the cylinder axis along the velocity direction), as evidenced by the equatorial peaks observed at q^* and $\sqrt{3}q^*$ in Fig. 7(a). The epitaxial transformation of these shear-aligned cylinders leads to the degenerate twinned bcc structure, as evidenced by the presence of four intense reflections at q^* positioned at 35° to the shear direction and the observation of higher-order reflections at $\sqrt{2}q^*$ that are approximately 55° to the shear direction.[27] We monitor the temporal evolution of the cylinder to sphere transition in Figs. 7(c) and 7(d) by tracking the intensities corresponding to the first Bragg reflection (q^*) of the cylindrical and spherical structures, as detailed previously.[10] The intensities at q^* corresponding to the parallel aligned cylinders (i.e., along the equatorial direction) and those corresponding to the spheres (i.e., at 35° to the meridional plane) are reported in Figs. 7(c) and 7(d). These intensities shown in Figs. 7(c) and 7(d) are normalized by the intensity along the meridional plane, which remains roughly constant throughout the transformation process. As expected from the rheological measurements [Fig. 6(b)], the addition of the filler does not lead to any significant changes in the kinetics of the order–order transition of aligned cylinders to spherical microdomains arranged on a bcc lattice. Further, the SANS data indicate that there is no alteration in the epitaxial relationship between the cylindrical and spherical microdomains as a result of the added layered silicate.

The influence of the silicate layers on the ordered structure of the cylindrical and spherical microdomains is examined by TEM on the samples quenched after melt rheology

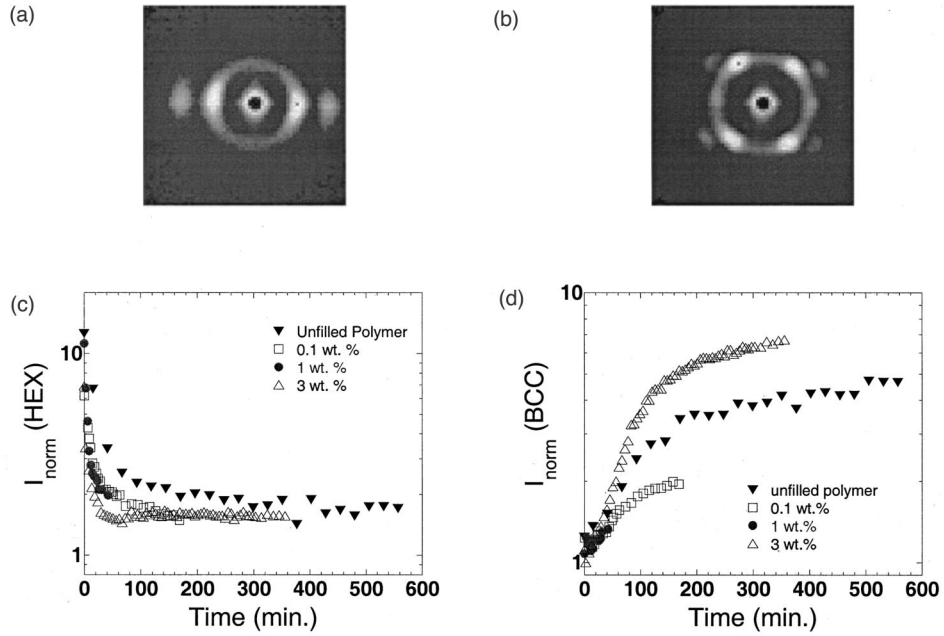

FIG. 7. Two-dimensional SANS patterns, with a neutron beam parallel to the velocity gradient direction [(a) and (b)], obtained for the well-oriented cylindrical microdomains, prepared by *in situ* application of large-amplitude reciprocating shear (a strain rate $|\dot{\gamma}| = 10\ s^{-1}$, $\gamma_0 = 2$, $T = 130\ °C$), and the corresponding epitaxially grown degenerate twinned spherical microdomains ($T = 150\ °C$, under quiescent conditions). The temporal evolution of the scattered intensity at the primary peak position q^* corresponding to the cylindrical structure (c) (the average of intensities along the equatorial plane) and that corresponding to the spherical microdomains (d) (the average of intensities at 35° to the shear direction or meridian) are normalized by the intensities along the meridional plane. The SANS data suggest that the kinetics are unaffected by the presence of the filler and are similar to rheological data obtained on shear-aligned samples.

and described in Figs. 3 and 4. Representative micrographs of the 1 wt.% hybrid annealed at 120 °C (cylindrical microdomains) and 150 °C (spherical microdomains) are shown in Fig. 8. The mesoscopic ordering of the spherical microdomain [Fig. 8(a)] appears to be strongly influenced by the silicate layers, with the layers acting as nucleation sites for the preferred PS rich spherical microphase. In fact, it appears that the PS can either coat the silicate sheets in the form of a layer or form hemispheres on the surface, with long-range order preserved from the surface. The ceramic layers provide scaffolding for the long-range ordering of spherical microdomains over several microns; whereas the cylindrical microdomains of PS [Fig. 8(b)] show essentially no templating at the silicate layers and, in fact, the long-range three-dimensional order appears to be disrupted by the presence of the silicate layers. We note that the micrograph for the cylindrical microdomains [Fig. 8(b)] is quite different from that observed for the unfilled cylindrical state reported in Ref. 11, where the cylindrical microdomains were shown to be short wormlike structures. Alternate explanations for the differences in the role of silicate layers on the development of spherical and cylindrical microdomain structures, such as the preferential segregation of the diblock or triblock and the differences in ordering behavior with architecture are ruled out on the basis of the results presented in the Appendix, the extremely low volume fraction at which the kinetic effects for spherical microdomains with bcc ordering saturate and the absence of visual and neutron scattering evidence that might indicate such a partitioning and lack of homogeneity in the filled hybrids.

CONCLUDING REMARKS

On the basis of the rheological, SANS, and TEM measurements shown, the highly anisotropic silicate layers of montmorillonite are seen to have a strong effect on the growth of spherical microdomains with cubic symmetry starting from an initially disordered state or from unaligned cylinders. Conversely, the kinetics for the development of unaligned anisotropic cylindrical microdomains from the disordered state appears to be unaffected (or even slightly disrupted) by the silicate layers. It is our contention that the development of mesoscopically ordered microdomains is critically dependent on the availability of a well-defined three-dimensional templating agent capable of preserving the long-range order over several multiples of the lattice dimensions. For this reason, we observed that starting from shear oriented cylinders, the presence of silicate layers has no influence on the kinetics and the pathway for the development of spherical microdomains. Further, to template micron length cylinders or lamellas would require nucleating surfaces whose leading dimensions are considerably larger than a micron, as has been observed in the surface-induced ordering of block copolymer lamellas and cylinders by bulk substrates and semi-infinite patterned surfaces.[28]

This contention of templating (as opposed to simple heterogeneous nucleation) is further supported by recent measurements (reported in the following paper) on the kinetics of spherical microdomain growth with three different layered silicates having platelet dimensions of 30 nm, 0.5–1μm, and 10 μm.[12] No templating of the spherical microdomains is observed for the 30 nm platelet hybrids. However, for the hybrids with the larger diameter platelets, strong templating and accelerated formation of the spherical microdomains are observed. These results reinforce the requirement of large length scale templating by the filler to observe enhanced growth kinetics and significant mesoscopic influence of the filler on the development of templated nanostructures.

ACKNOWLEDGMENTS

The authors thank J. Ren and M. A. Modi for help with a sample preparation and J. Ball for the TEM measurements. Useful discussions with Professor Balsara, Professor Colby,

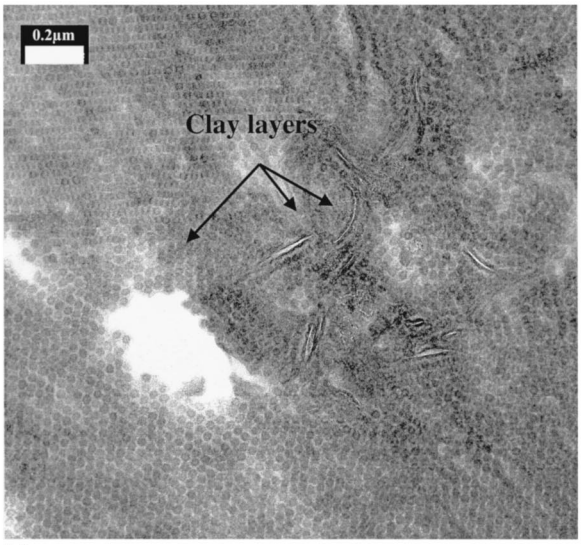

(a)

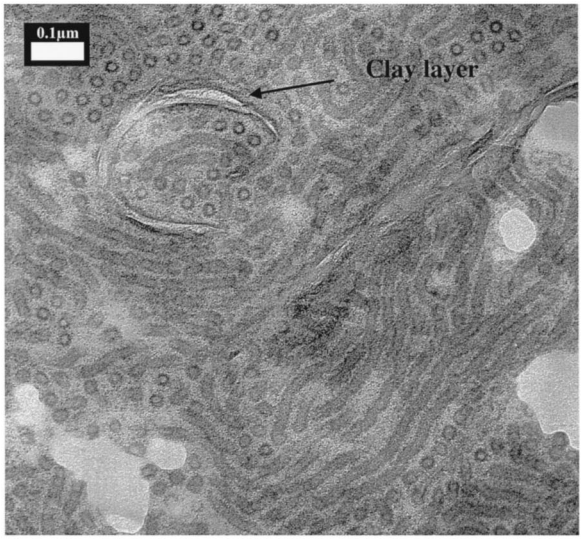

(b)

FIG. 8. Transmission electron micrographs exhibiting the influence of the addition of 1 wt.% layered silicate (2C18M) on the spherical and cylindrical structures evolved at 150 °C and 120 °C [(a) and (b), respectively]. The sections were stained with RuO_4, preferentially absorbed by polystyrene and seen as dark regions in the micrographs. The long-range order of the spherical microdomain structure is templated by the silicate layers and this nucleation event is thought to cause the enhanced kinetics observed in the rheological measurements shown in Fig. 3. Conversely, the long-range order of the cylindrical structure appears to be disturbed due to the presence of the silicate layers and leads to the presence of highly disoriented cylindrical microdomains.

Professor Giannelis, Professor Green, Professor Kornfield, Professor Kumar, and Professor Manias, and Dr. Chapman, Dr. Karim, and Dr. Vaia are gratefully acknowledged. The authors would like to especially thank Dr. Hammouda of NIST for extensive help with the neutron scattering measurements. Partial funding support from the National Science Foundation (NSF) (DMR-9875321) and Texas coordinating board (ATP) is gratefully acknowledged. This work made use of TCSUH/MRSEC Shared Facilities supported by the State of Texas through TCSUH and by the NSF (DMR-9632667). The SANS measurements conducted at NIST were supported by the National Science Foundation under Agreement No. DMR-9986442.

TABLE I. Characterization of the phase transitions.

Sample	% Triblock	T_{ODT}[a]	T_{ODT}[b]	T_{OOT}[b]
Triblock	93	199±2 °C	198±3 °C	136±2 °C
Diblock	14	192±2 °C	192±3 °C	143±3 °C
Blend	65	196±2 °C	195±5 °C	138±3 °C

[a] T_{ODT} determined by SANS measurements and shown in Fig. 10.
[b] T_{ODT} and T_{OOT} determined by linear viscoelastic measurements using isochronal plots at zero heating rate as shown in Fig. 9 and from detailed frequency scans for well-equilibrated structures.

APPENDIX: INFLUENCE OF BLENDING ON THERMODYNAMIC BEHAVIOR

The sample used in this study is a blend of a matched diblock and triblock copolymer, with ~65% triblock. In this appendix we show that for the case of PS–PEB block copolymers, the effect of architecture has a relatively small effect on the location of the thermodynamic phase transitions and is consistent with an architecture-independent Flory–Huggins thermodynamic interaction parameter $[\chi(T)]$ with a strong temperature dependence of $\chi(T)$.[10,29]

Based on SAXS measurements, Ijichi and co-workers[30] have suggested that for the styrene–isoprene system, $\chi(T)$ is a strong function of block architecture. On the other hand, Balsara and co-workers[31] using SANS have suggested that the thermodynamic interaction parameter χ for the styrene–isoprene system is within the errors of the experiment independent of the molecular architecture of the block copolymer (i.e., similar for diblock and triblock copolymers and independent of the composition of the block copolymer). Similarly, Register and co-workers,[32] Bates and co-workers,[33] and Lodge and co-workers[34] have shown that a single architecture-independent χ parameter adequately describes the phase behavior of diblock, triblock, and mixtures of di- and triblock copolymers. To clarify the situation for the current case we examined the effect of blending diblock and triblock copolymers on the microphase behavior for the S-EB system.

We prepared diblock and triblock fractions by successive solvent (toluene and cyclohexane) solubilization and nonsolvent (methanol) precipitation, as described previously.[35] A detailed characterization of the different fractions studied as obtained by gel permeation chromatography (Waters 150C with four Polymer Laboratories columns of 10^5, 10^4, 10^3, and 500 Å pore size and equipped with UV and RI detection; THF as eluent; $T=30$ °C; and the flow rate of 1 ml/min) is provided in Table I. The location of the order–disorder transition (T_{ODT}) is studied by melt-state linear viscoelastic measurements and by quiescent state SANS measurements. The location of the cylinder-to-sphere order–order transition (T_{OOT}) is examined by linear viscoelastic measurements.

The order–disorder and order–order transition as studied by linear viscoelastic measurements and shown in terms of an isochronal plot at a low frequency of 0.04 rad/s is shown

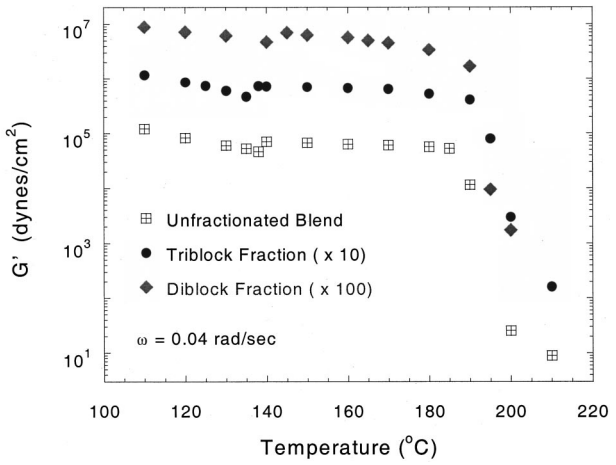

FIG. 9. Isochronal plot of G' vs temperature for the unfractionated blend (studied in this paper), the fractionated triblock, and the fractionated diblock. The plot was prepared from frequency scans performed on well-equilibrated samples, sometimes equilibrated for as long as 24 h at a fixed temperature. The data for the triblock and diblock are scaled in order to distinguish between the different datasets. For all three samples, there is a slight increase in G' upon traversing the T_{OOT}. The T_{ODT} is accompanied by a precipitous drop in G' and detailed assignment of T_{ODT} provided in Table I was performed by examining the frequency scans (Ref. 11).

in Fig. 9. The isochronal plots were prepared from frequency scans on well-equilibrated samples (i.e., an effective zero heating rate), sometimes equilibrated for over 24 h at a temperature to attain equilibrium values.[9,11] The order–disorder transition for the triblock, diblock, and the mixture used in this study was also examined by SANS measurements under quiescent conditions and shown in Fig. 10. The temperature corresponding to the *order–order* transition temperature was not investigated by SANS measurements because of the long time required to attain equilibrium.

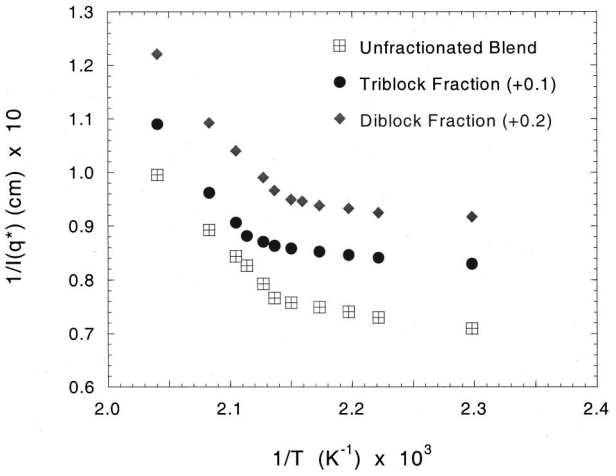

FIG. 10. Temperature dependence of the SANS intensity at q^*, corresponding to the primary intensity peak for the block copolymer, for the unfractionated blend, the fractionated triblock, and the fractionated diblock. The T_{ODT} is identified by the location of the discontinuity in the intensity. Samples were prepared by heating to the isotropic state and then quenched to 162 °C and allowed to equilibrate for ~24 h. All the data presented in this figure were obtained during the heating of the samples from the ordered state to the disordered state.

The thermal transitions as determined by the viscoelastic and SANS measurements are summarized in Table I. The triblock copolymer exhibits a slightly higher T_{ODT} as compared to the diblock copolymer is and consistent with previous experiments[32–34] and theoretical predictions.[36] On the other hand, the T_{OOT} for the triblock is slightly lower than that of the diblock copolymer, contrary to the previous results of Ryu *et al.* on PS–PI diblock and triblock copolymers.[34] It is conceivable that the increased temperature dependence of χ for the PS–PEB systems as compared to PS–PI, and a significantly different conformational asymmetry[37] with a more pronounced temperature dependence could be responsible for the differences in behavior for the PS–PEB system in comparison to the PS–PI system. Most importantly, however, at 120 °C all three samples (diblock, triblock, and the blend examined in this study) formed cylindrical microdomains, while at 150 °C all three samples formed spherical microdomains.

[1] G. H. Fredrickson and F. S. Bates, Annu. Rev. Mater. Sci. **26**, 501 (1996).
[2] H. E. Warriner, S. H. J. Idziak, N. L. Slack, P. Davidson, and C. R. Safinya, Science **271**, 969 (1996).
[3] S. S. Kim, W. Zhang, and T. J. Pinnavaia, Science **282**, 1302 (1998); B. D. Discher, Y.-Y. Won, D. S. Ege, J. C.-M. Lee, F. S. Bates, D. E. Discher, and D. A. Hammer, *ibid.* **284**, 1143 (1999).
[4] E. P. Giannelis, R. Krishnamoorti, and E. Manias, Adv. Polym. Sci. **138**, 107 (1999).
[5] S. A. Jenekhe and X. L. Chen, Science **283**, 372 (1999); S. A. Jenekhe and X. L. Chen, *ibid.* **279**, 1903 (1998); S. I. Stupp and P. B. Braun, *ibid.* **277**, 1242 (1997); S. I. Stupp, V. LeBonheur, K. Walker, L. S. Li, K. E. Huggins, M. Keser, and A. Amstutz, *ibid.* **276**, 384 (1997).
[6] D. Zhao, J. Feng, Q. Huo, N. Melosh, G. H. Fredrickson, B. F. Chmelka, and G. D. Stucky, Science **279**, 548 (1998); K. M. McGrath, D. M. Dabbs, N. Yao, I. A. Aksay, and S. M. Gruner, *ibid.* **277**, 552 (1997).
[7] K. Kageyama, J.-I. Tamazawa, and T. Aida, Science **285**, 2113 (1999).
[8] B. K. G. Theng, *Formation and Properties of Clay Polymer Complexes* (Elsevier, New York, 1979).
[9] R. Krishnamoorti, M. A. Modi, M. F. Tse, and H.-C. Wang, Macromolecules **33**, 3810 (2000).
[10] R. Krishnamoorti, A. S. Silva, M. A. Modi, and B. Hammouda, Macromolecules **33**, 3803 (2000).
[11] M. A. Modi, R. Krishnamoorti, M. F. Tse, and H.-C. Wang, Macromolecules **32**, 4088 (1999).
[12] R. Krishnamoorti, A. S. Silva, and C. A. Mitchell, J. Chem. Phys. **115**, 7175 (2001), following paper.
[13] J. Ren, A. S. Silva, and R. Krishnamoorti, Macromolecules **33**, 3739 (2000); J. Chem. Phys. **114**, 4968 (2000).
[14] M. F. Tse, H.-C. Wang, T. D. Shaffer, M. C. McElrath, M. A. Modi, and R. Krishnamoorti, Polym. Eng. Sci. **40**, 2182 (2000).
[15] K. A. Koppi, M. Tirrell, F. S. Bates, K. Almdal, and K. Mortensen, J. Rheol. **38**, 999 (1994).
[16] K. A. Koppi, M. Tirrell, F. S. Bates, K. Almdal, and R. H. Colby, J. Phys. II **2**, 1941 (1993).
[17] R. A. Vaia and E. P. Giannelis, Macromolecules **30**, 8000 (1997).
[18] R. A. Vaia and E. P. Giannelis, Macromolecules **30**, 7990 (1997).
[19] V. V. Ginzburg and A. C. Balazs, Macromolecules **32**, 5681 (1999); A. C. Balazs, C. Singh, and E. Zhulina, *ibid.* **31**, 8370 (1998).
[20] R. Krishnamoorti, C. A. Mitchell, and A. S. Silva (unpublished).
[21] J. L. Adams, D. J. Quiram, W. W. Graessley, R. A. Register, and G. A. Marchand, Macromolecules **29**, 2929 (1996).
[22] G. Floudas, N. Hadjichristidis, M. Stamm, A. E. Likhtman, and A. N. Semenov, J. Chem. Phys. **106**, 3318 (1997).
[23] R. G. Larson, K. I. Winey, S. S. Patel, H. Watanabe, and R. Bruinsma, Rheol. Acta **32**, 245 (1993); T. Hashimoto, T. Ogawa, N. Sakamoto, M. Ichimiya, J. K. Kim, and C. D. Han, Polymer **39**, 1573 (1998).
[24] N. S. Enikolopyan, M. L. Fridman, I. O. Stalnova, and V. L. Popov, Adv. Polym. Sci. **96**, 1 (1990).
[25] G. W. Brindley and G. Brown, *Crystal Structure of Clay Minerals and their X-Ray Identification* (Mineralogical Society, London, 1980).

[26] G. J. A. Sevink, A. V. Zvelindovsky, B. A. C. van Vlimmeren, N. M. Maurits, and J. G. E. M. Fraaije, J. Chem. Phys. **110**, 2250 (1999).
[27] M. F. Schulz, F. S. Bates, K. Almdal, and K. Mortensen, Phys. Rev. Lett. **73**, 86 (1994).
[28] S. H. Anastasiadis, T. P. Russell, S. K. Satija, and C. F. Majkrzak, Phys. Rev. Lett. **62**, 1852 (1989); P. Green, T. M. Christensen, and T. P. Russell, Macromolecules **24**, 252 (1991); P. Lambooy, T. P. Russell, G. J. Kellogg, A. M. Mayers, P. D. Gallagher, and S. K. Satija, Phys. Rev. Lett. **72**, 2899 (1994); A. M. Mayes, T. P. Russell, V. R. Deline, S. K. Satija, and C. F. Majkrzak, Macromolecules **27**, 7447 (1994); L. Rockford, Y. Liu, P. Mansky, T. P. Russell, M. Yoon, and S. G. J. Mochrie, Phys. Rev. Lett. **82**, 2602 (1999).
[29] L. J. Adams, D. J. Quiram, W. W. Graessley, and R. A. Register, Macromolecules **31**, 201 (1998).
[30] Y. Ijichi, T. Hashimoto, and L. J. Fetters, Macromolecules **22**, 2817 (1989).
[31] C. C. Lin, S. V. Jonnalagadda, P. K. Kesani, H. J. Dai, and N. P. Balsara, Macromolecules **27**, 7769 (1994).
[32] L. J. Adams, W. W. Graessley, and R. A. Register, Macromolecules **27**, 6026 (1994).
[33] M. D. Gehlsen, K. Almdal, and F. S. Bates, Macromolecules **25**, 939 (1992).
[34] C. Y. Ryu, M. S. Lee, D. A. Hajduk, and T. P. Lodge, J. Polym. Sci. Part B: Polym. Phys. **35**, 2811 (1997).
[35] D. A. Hajduk, S. M. Gruner, P. Rangarajan, R. A. Register, L. J. Fetters, C. Honecker, R. J. Albalak, and E. L. Thomas, Macromolecules **26**, 490 (1994).
[36] A. M. Mayes and M. J. Olvera de la Cruz, J. Chem. Phys. **91**, 7228 (1989).
[37] M. W. Matsen and F. S. Bates, J. Polym. Sci. Part B: Polym. Phys. **35**, 945 (1997).